

Formation, nature, and stability of the arsenic-silicon-oxygen alloy for plasma doping of non-planar silicon structures

Peter L. G. Ventzek, Kyoung E. Kweon, Hirokazu Ueda, Masahiro Oka, Yasuhiro Sugimoto, and Gyeong S. Hwang

Citation: *Applied Physics Letters* **105**, 262102 (2014); doi: 10.1063/1.4905206

View online: <http://dx.doi.org/10.1063/1.4905206>

View Table of Contents: <http://scitation.aip.org/content/aip/journal/apl/105/26?ver=pdfcov>

Published by the [AIP Publishing](#)

Articles you may be interested in

[Mechanisms for dose retention in conformal arsenic doping using a radial line slot antenna microwave plasma source](#)

J. Appl. Phys. **117**, 224904 (2015); 10.1063/1.4922412

[Conformal doping of topographic silicon structures using a radial line slot antenna plasma source](#)

J. Appl. Phys. **115**, 214904 (2014); 10.1063/1.4881075

[Boron- and phosphorus-doped silicon germanium alloy nanocrystals—Nonthermal plasma synthesis and gas-phase thin film deposition](#)

APL Mat. **2**, 022104 (2014); 10.1063/1.4865158

[Plasma process optimization for N-type doping applications](#)

AIP Conf. Proc. **1496**, 67 (2012); 10.1063/1.4766491

[A density functional theory study of the atomic structure, formation energy, and vibrational properties of nitrogen-vacancy-oxygen defects in silicon](#)

J. Appl. Phys. **108**, 033513 (2010); 10.1063/1.3387912

An advertisement for Edmund Optics. On the left, a man in a blue shirt is smiling and looking at a piece of laboratory equipment. The background is dark with a grid pattern. The text is in yellow and white. A blue banner in the top right corner says 'HURRY! FINAL WEEKS TO APPLY'. The main text reads 'NEED FREE PRODUCTS FOR YOUR LAB?'. Below that, it says '• 45 Global Educational Awards Available'. At the bottom, there is a website URL 'www.edmundoptics.com/award', a button that says 'APPLY NOW! TAKES ONLY 6 MINUTES.', and the Edmund Optics logo with the tagline 'Edmund optics | worldwide'.

Formation, nature, and stability of the arsenic-silicon-oxygen alloy for plasma doping of non-planar silicon structures

Peter L. G. Ventzek,^{1,a),b)} Kyoung E. Kweon,^{2,b)} Hirokazu Ueda,³ Masahiro Oka,³ Yasuhiro Sugimoto,³ and Gyeong S. Hwang^{2,a),b)}

¹Tokyo Electron America, Inc., Austin, Texas 78741, USA

²Department of Chemical Engineering, University of Texas at Austin, Austin, Texas 78712, USA

³Tokyo Electron Ltd., Nirasaki, Yamanashi 407-0192, Japan

(Received 23 November 2014; accepted 17 December 2014; published online 30 December 2014)

We demonstrate stable arsenic-silicon-oxide film formation during plasma doping of arsenic into non-planar silicon surfaces through investigation of the nature and stability of the ternary oxide using first principles calculations with experimental validations. It is found that arsenic can be co-mingled with silicon and oxygen, while the ternary oxide exhibits the minimum energy phase at $x \approx 0.3$ in $\text{As}_x\text{Si}_{1-x}\text{O}_{2-0.5x}$. Our calculations also predict that the arsenic-silicon-oxide alloy may undergo separation into As-O, Si-rich As-Si-O, and Si-O phases depending on the composition ratio, consistent with experimental observations. This work highlights the importance of the solid-state chemistry for controlled plasma doping. © 2014 AIP Publishing LLC.

[<http://dx.doi.org/10.1063/1.4905206>]

Logic structures for the 14 nm node include topographic gate structures (e.g., FinFETs) that must be conformally doped. Ultra shallow junction depths required for planar MOS gate technologies have been met by conventional ion implantation¹ or plasma source ion implantation^{2,3} (PSII) technology. PSII² relies on the existence of the plasma sheath rendering dopant ion trajectories normal to a surface making conformality problematic. 45° beam implant is difficult for topographic gate structures with high aspect ratio (AR) spacing between them (i.e., $\text{AR} > 1$).

Plasma doping technology has emerged as a viable method for conformal doping. Initial demonstrations of plasma doping were PSII processes with pressures at which ion scattering was invoked to explain the conformality.⁴⁻⁷ Sidewall ion impacts are essential for plasma doping but, as is for atomic layer deposition, self-limiting processes are needed for true conformality.⁸ Plasma doping starts with the injection of a molecular dopant precursor (e.g., AsH_3) into a plasma which dissociates it, releasing the dopant (e.g., As). Dopants diffuse into the thin amorphous layer formed on the Si substrate. Si and oxygen (O) are co-deposited and the dopant driven to saturation in the interface of the amorphous and overlying oxide layer. Saturation is coincident with segregation.⁹⁻¹¹ Plasma doping is performed near room temperature; annealing activates infused dopants and evaporates excess protective material. Details of the plasma doping process are summarized by Ueda *et al.*¹¹

It is well known that a high-dose ion implantation may lead to dopant cluster formation and electrical deactivation.¹²⁻¹⁵ While dopant aggregation has been found to be mediated by point-like defects,^{13,14} defect formation and defect-dopant interaction have been rather well studied in bulk Si; for instance, Hwang and co-workers proposed routes

for defect-mediated As clustering in Si using first-principles calculations.¹⁵ However, little is known about the formation and structure of the ternary dopant-Si-O alloy despite its importance for a better understanding of the self-limiting processes in plasma doping.

While the ternary system associated with plasma doping has not been studied, there have been attempts to understand the impact of oxygen in classical implant. Post ion implant anneal studies in which annealing has been performed in oxygen environments show that activation and profile results strongly depend on oxygen exposure.^{16,17} Work by Kobayashi *et al.*⁹ and a more recent paper by Steen *et al.*¹⁰ note the segregation of implanted As to oxide-Si interfaces and the formation of donor states upon annealing. Numerous studies have investigated segregation when As is beam implanted through silicon oxide layers to underlying Si.¹⁸⁻²¹ These papers showed that As precipitates were observed to form and migrate. While the thickness of the oxide films is larger, the results of Celler *et al.*¹⁸ are similar to the observation of As-rich interfaces by Ueda *et al.*¹¹ These studies highlight the need to clarify the phase behavior of the mixed arsenic-silicon-oxide (As-Si-O) system.

This paper provides a first-principles-based description of the structure and stability of the amorphous As-Si-O system. Computations show that there is a preferred stoichiometry low concentration As dopant infused Si-O film. The existence of this preferred stoichiometry allows prediction of conditions where plasma doping is self-capping, i.e., a Si-O layer forms above a dosed sub-surface post anneal, such that the dose is self-limiting. Our first-principles study also shows that Si is unlikely to be absorbed into pure or As-rich oxides. Both scenarios are observed in experiments. These findings help to explain the self-limiting mechanism in conformal plasma doping.

Concentration depth profiles associated with arsenic plasma doping using a radial line slot antenna plasma source²² are included in Fig. 1 [Secondary Ion Mass Spectrometry (SIMS)]

^{a)} Authors to whom correspondence should be addressed. Electronic addresses: peter.ventzek@us.tel.com and gshwang@che.utexas.edu

^{b)} P. L. G. Ventzek, K. E. Kweon, and G. S. Hwang contributed equally to this work.

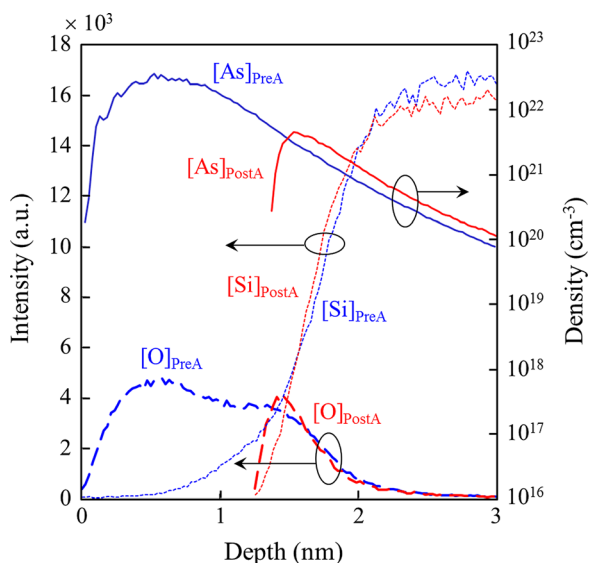
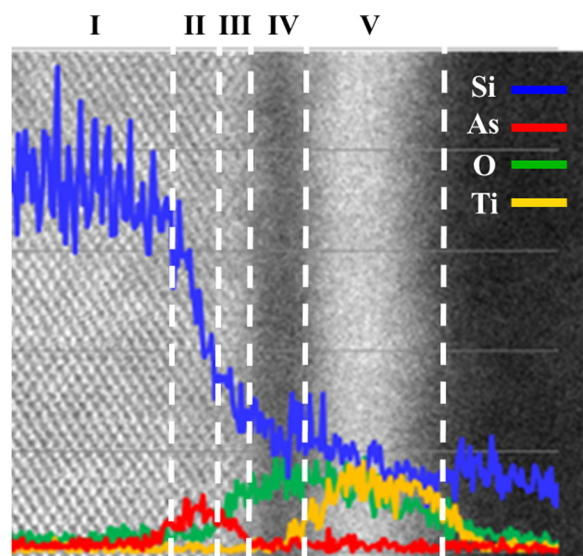


FIG. 1. SIMS depth profile of As, Si, and O concentrations due to plasma doping with 3000 W microwave power and an AsH_3 flowrate of 0.7 sccm diluted helium 999.3 sccm at 150 mTorr pre and post anneal at 950°C 120 s. The bias power was 450 W at 13.56 MHz.

and Fig. 2 [Transmission Electron Microscope–Energy Dispersive X-ray Spectroscopy (TEM-EDX)]. The microwave power in the radial line slot antenna source was 3000 W and the flow rate of arsine was 0.7 sccm diluted in 999.3 sccm helium with a process pressure of 150 mTorr. SIMS measured profiles for blanket wafer (fin top) doping are presented in Fig. 1 for both pre- and post-anneal conditions. Figure 2 is a TEM EDX measurement of the depth profile on a fin sidewall.

Noticeable in Fig. 1, for the pre-anneal condition, is the substantial As film at the surface above the Si substrate. Present in the film is an appreciable O amount. Si is evident but the oxide surface is effectively free of Si with the Si content increasing towards the oxide-Si substrate interface. Note



I: Fin II: Dosed Layer III: Mixed (As) Oxide
IV: Silicon Oxide V: Decoration

FIG. 2. TEM-EDX profiles of As, Si, O, and Ti (decoration layer) on a fin sidewall. The scale of the concentrations is arbitrary and sets to illustrate the relative locations maxima and minima of species concentrations.

that the As densities are plotted while Si and O are plotted in arbitrary units (counts). The As densities are normalized to $3 \times 10^{22} \text{cm}^{-3}$. The measured peak density values were approximately double and are an artifact of calibration. Post rapid thermal anneal at 950°C , the As-O film is removed leaving a thin As-O layer over a layer co-mingled with Si; we will refer to this case as the As-rich condition and show with a computational model of the material system that it is energetically unfavorable to add Si to this film.

The fin side-wall depth profile (Fig. 2) is markedly different. This, the post anneal condition, shows (a) crystalline Si (*c*-Si) substrate, (b) an As infused layer, (c) an As-Si-O layer, (d) a Si-O layer, and (e) a decoration layer. We will refer to this as the As-lean condition and show with a computational model of the material system that separation into distinct layers (Si-O, mixed As-Si-O) is energetically favorable. We use the term “As-lean” because the flux of As dopants to the sidewalls (relative to the top of the fin) is greatly reduced in higher aspect ratio trenches between fin structures.

First-principles density functional theory (DFT) calculations were performed to examine the formation and structure of the oxide films presented in Figs. 1 and 2. We employed the generalized gradient approximation with the Perdew-Burke-Ernzerhof exchange-correlation functional (GGA-PBE),²³ as implemented in the Vienna *Ab-initio* Simulation Package (VASP 5.2.2),²⁴ and the projected augmented wave²⁵ with a plane-wave basis set to describe the interaction between core and valence electrons. For geometry optimization and electronic structure calculations, we used an energy cutoff of 500 eV for the plane wave expansion of one-electronic eigenfunctions and a gamma-centered $(2 \times 2 \times 2)$ Monkhorst-Pack *k*-point mesh²⁶ was used for Brillouin zone sampling. All model geometries were optimized using a conjugated gradient method until the residual forces on constituent atoms become smaller than $0.02 \text{ eV}/\text{\AA}$.

It is well known that arsenic trioxide can be formed via oxidation of arsenic and arsenic containing minerals. In the gas and liquid phases, arsenic trioxide may preferentially exist in the form of As_4O_6 ; however, it can significantly dissociate into As_2O_3 , as illustrated in Fig. 3; our DFT calculation predicts the former to be about 2.0 eV (per As_2O_3 unit) more favorable than the latter. In the solid state, three different forms have been reported,^{27,28} such as molecular (i.e., discrete As_4O_6 cages in arsenolite²⁹) and two polymeric (i.e., As_2O_3 layers in claudetite I³⁰ and II³¹) forms (see Fig. 3). In the arsenic oxide polymorphs, each As atom is surrounded by three O atoms while containing a lone electron pair, forming a tetrahedron with stoichiometry of $\text{AsO}_{1.5}$. We also generated cross-linked amorphous arsenic oxide (*a*- As_2O_3) structures, similar to the case of amorphous silicon oxide (*a*- SiO_2), using *ab initio* molecular dynamics (AIMD) with a periodic supercell containing 10 As_2O_3 units (=50 atoms) (see Refs. 32 and 33 for a detailed description of the amorphous structure generation). It is reasonable to expect that arsenic may be oxidized where oxygen to reach the substrate; then, the arsenic oxide layer would likely remain in the amorphous phase especially in the presence of ion bombardment. According to our dispersion-corrected DFT calculations, the *a*- As_2O_3 structure (with a density ρ of 3.74 g/cm^3)²⁸ is predicted to be only about 0.1 eV (per $\text{AsO}_{1.5}$ unit)

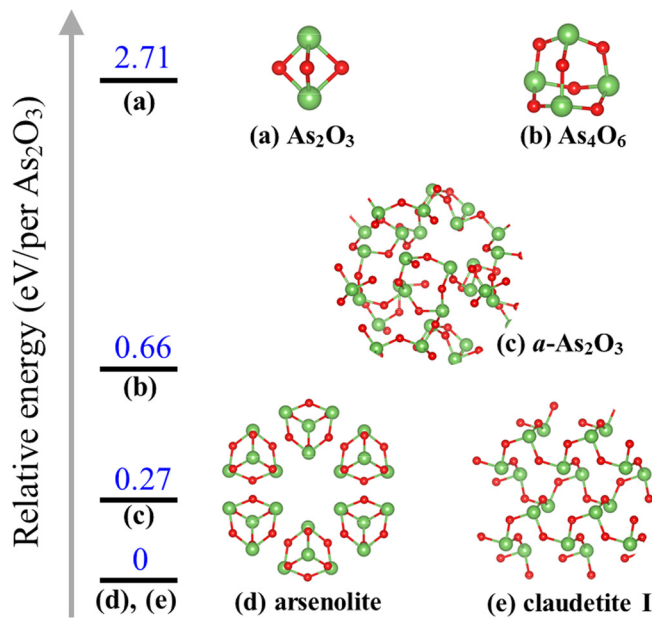


FIG. 3. Atomic configurations and relative formation energies of arsenic trioxide in various forms of interest; (a) As_2O_3 cluster, (b) As_4O_6 cluster, (c) bulk amorphous As_2O_3 ($a\text{-As}_2\text{O}_3$), (d) arsenolite, and (e) claudetite I. The green and red balls indicate As and O atoms, respectively.

less favorable than the (most stable) arsenolite structure (with $\rho = 3.87 \text{ g/cm}^3$).²⁹ The structure of $a\text{-SiO}_2$ was also generated using AIMD with a 60-atom (=20 SiO_2 units) cubic supercell at $\rho = 2.2 \text{ g/cm}^3$; the strain energy of $a\text{-SiO}_2$ with respect to crystalline α -quartz is estimated to be about 0.3 eV (per SiO_2 unit), in good agreement with the previous theoretical predictions.³⁴

To explore the structure and relative stability of the As-Si-O system, we generated and compared the amorphous oxide structures by varying the As to Si ratio (x in $\text{As}_x\text{Si}_{1-x}\text{O}_{2-0.5x}$); the structures were fully relaxed using AIMD. Figure 4 shows a variation in the relative energy (ΔE) for $a\text{-As}_x\text{Si}_{1-x}\text{O}_{2-0.5x}$ as a function of x with respect to pure $a\text{-SiO}_2$ and $a\text{-As}_2\text{O}_3$. Here, $\Delta E_{\text{tot}} = E(a\text{-As}_x\text{Si}_{1-x}\text{O}_{2-0.5x}) - xE(a\text{-As}_2\text{O}_3)/2 - (1-x)E(a\text{-SiO}_2)$, where $E(M)$ is the total energy per unit of system M (= $\text{As}_x\text{Si}_{1-x}\text{O}_{2-0.5x}$, $a\text{-As}_2\text{O}_3$, and $a\text{-SiO}_2$). In the calculations, the ρ of $\text{As}_x\text{Si}_{1-x}\text{O}_{2-0.5x}$ was approximated using linear interpolation between $\rho(a\text{-As}_2\text{O}_3)$ and $\rho(a\text{-SiO}_2)$, i.e., $\rho(\text{As}_x\text{Si}_{1-x}\text{O}_{2-0.5x}) = x\rho(a\text{-As}_2\text{O}_3) + (1-x)\rho(a\text{-SiO}_2)$. The calculation results show that ΔE_{tot} decreases (increases) as a small amount of As (Si) is added to the $a\text{-SiO}_2$ ($a\text{-As}_2\text{O}_3$) matrix, while exhibiting the minimum and maximum values at $x=0.3$ and 0.8, respectively. This suggests that As can be favorably incorporated into the $a\text{-SiO}_2$ ($a\text{-As}_2\text{O}_3$) matrix, while exhibiting the minimum and maximum values at $x=0.3$ and 0.8, respectively. This suggests that As can be favorably incorporated into the $a\text{-SiO}_2$ matrix to form an As-Si-O film (up to the As to Si ratio of $x=0.3$); on the other hand, Si addition to the $a\text{-As}_2\text{O}_3$ matrix tends to be unfavorable energetically. Our calculations also demonstrate that the As-Si-O system undergoes phase separation as the As and Si concentrations become comparable (see the corresponding atomic structure in Fig. 4); this could provide an explanation for the aforementioned experimental observation of As- and Si-rich regions in the As-Si-O thin film (Fig. 2).

To better understand the oxidation behavior, we looked at the relative contributions of possible strain and electronic effects (associated with the changes in lattice distortions and

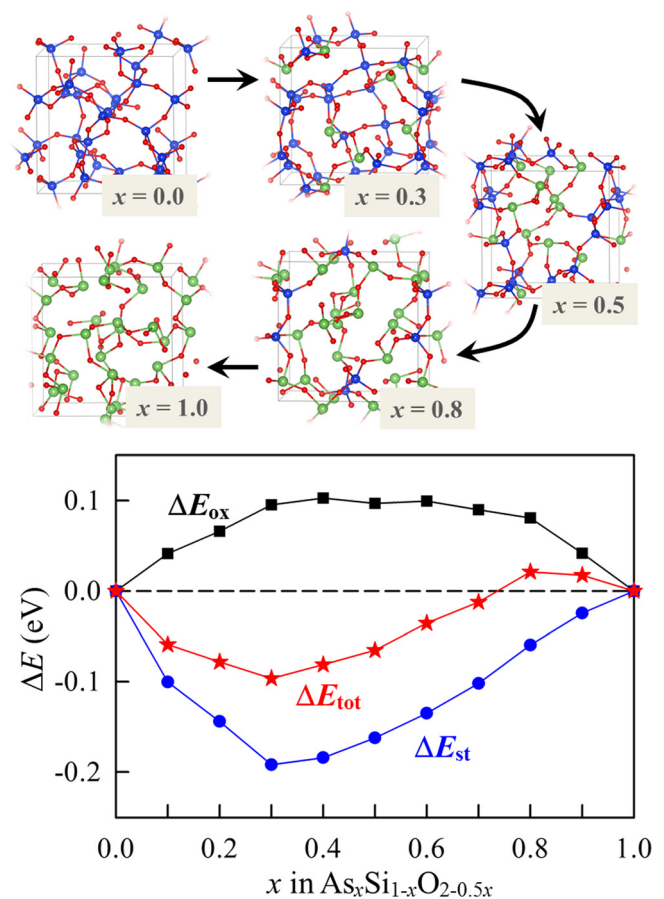


FIG. 4. Relative total (ΔE_{tot}), strain (ΔE_{st}), and penalty (ΔE_{ox}) energies for $a\text{-As}_x\text{Si}_{1-x}\text{O}_{2-0.5x}$ as a function of x with respect to pure $a\text{-SiO}_2$ and $a\text{-As}_2\text{O}_3$. Selected $a\text{-As}_x\text{Si}_{1-x}\text{O}_{2-0.5x}$ structures are also shown; the blue, green, and red balls represent Si, As, and O atoms, respectively.

oxidation states, respectively). That is, ΔE_{tot} is decoupled in terms of the changes in strain energy (ΔE_{st}) and oxidation penalty energy (ΔE_{ox}), $\Delta E_{\text{tot}} = \Delta E_{\text{st}} + \Delta E_{\text{ox}}$. The penalty energy represents an increase in the As-O and Si-O bond energies arising from various As/Si oxidation states. Our DFT calculations show that there is a charge transfer from As to Si through an As-O-Si linkage; hence, compared to the pure As_2O_3 and SiO_2 cases, As and Si atoms in the As-Si-O system are, respectively, more and less oxidized, as the nearest As/Si atoms are replaced by dissimilar atoms. The predicted oxidation states and penalty energies of As and Si atoms for different bonding environments are summarized in Table I; the strain-free clusters used in the calculations are presented in Fig. S1.³⁵ From a given As-Si-O structure, ΔE_{ox} is obtained by adding the energy penalties of particularly oxidized As and Si atoms, and ΔE_{st} is estimated by subtracting ΔE_{ox} from ΔE_{tot} .

Inspecting Fig. 4, it can be observed that ΔE_{ox} increases as As is added to the $a\text{-SiO}_2$ matrix but is more than offset by the decrease in strain. The existence of a minimum in ΔE_{tot} for relatively small amounts of As added to the $a\text{-SiO}_2$ system suggests that the formation of an As-Si-O mixed film with 30 at. % As is highly probable. Another feature in Fig. 4 is that at high As content in the mixed phase film, the reduction in ΔE_{st} is unable to off-set the ΔE_{ox} and the ΔE_{tot} increases. This implies that once formed, an As-O phase is unlikely to accept additional Si.

TABLE I. Predicted oxidation states based on Bader charge analysis and corresponding penalty energies (ΔE_{ox}) for Si (upper) and As (lower) in the As-Si-O system, the cluster models.

	Number of As neighbors for Si				
	0	1	2	3	4
oxidation state	+3.211	+3.200	+3.185	+3.170	+3.157
ΔE_{ox} (eV)	0	0.070	0.127	0.207	0.306
	Number of Si neighbors for As				
	0	1	2	3	
oxidation state	+1.639	+1.669	+1.696	+1.728	
ΔE_{ox} (eV)	0	0.010	0.107	0.211	

Our calculation results can be related to the experimental observations in Figs. 1 and 2. First, as shown in Fig. 1, the As-O layer, previous to being annealed (PreA), has little to no Si present in it. This could be explained by the prediction that addition of small amounts of Si to an As-O layer is not energetically favored as ΔE_{tot} increases both due to ΔE_{st} and ΔE_{ox} ; this is arrived at by starting at the pure $\alpha\text{-As}_2\text{O}_3$ side in Fig. 4 and moving to the left (i.e., from 100 at. % to 90 at. % As). The As-O layer has been found to sublime at typical annealing temperatures, and thus what remains at the surface post-anneal is a mixed As-Si-O phase.¹¹

Second, Fig. 2 shows a distinct As-Si-O layer (layer III) that forms via As mixing with the Si-O film. This can be understood by starting at the left hand side of the relative formation energy plot in Fig. 4 and moving to the right (i.e., from 0 at. % to ~30 at. % As); the existence of a minimum energy composition confirms that the As-Si-O film formation is energetically favorable. It is also worthwhile to point out that, in both the As-rich (Fig. 1) and As-lean (Fig. 2) cases, the energetically favored ternary As-Si-O film abuts an As infused Si layer; the atomic-level description of the interface structure would help to better understand the underlying mechanisms for plasma doping.

In summary, first-principles DFT calculations with experimental validations were carried out to examine the formation, nature, and stability of ternary As-Si-O films during As plasma doping of non-planar Si surfaces. The relative stability of the ternary oxide was analyzed in terms of the changes in strain energy (ΔE_{st}) and oxidation penalty energy (ΔE_{ox}) relative to the pure $\alpha\text{-As}_2\text{O}_3$ and $\alpha\text{-SiO}_2$ structures. We find that adding small amounts of As to pure $\alpha\text{-SiO}_2$ sees a decrease in ΔE_{st} that more than off-sets the increase in ΔE_{ox} . The result is a favored film with a minimum formation energy with an As atom fraction of 0.3 with the Si atom fraction being 0.7 in the fully oxidized film, i.e., $x = 0.3$ in $\text{As}_x\text{Si}_{1-x}\text{O}_{2-0.5x}$. On the other hand, adding Si to an $\alpha\text{-As}_2\text{O}_3$ film is not energetically favored as both ΔE_{st} and ΔE_{ox} increase. This suggests that a fully oxidized As_2O_3 layer may not absorb Si and the any added deposition of Si and O would be expected to form an overlying Si-O film. When the amounts of Si and As are comparable, the ternary oxide may undergo separation into As-O and Si-rich As-Si-O phases.

Our calculations results are consistent with experimental observations. First, the case of As addition to an $\alpha\text{-SiO}_2$ layer

is important in that where oxygen present in the plasma doping of a pristine Si surface As would see an oxidized layer at the very start of the process. Incoming As atoms would be mixed with the Si-O layer to form an As-Si-O layer (perhaps with an As-O interlayer between the underlying Si substrate and the As-Si-O layer, depending on As dose); this is observed in the As-lean case (see Fig. 2). Second, it is not favored to add Si atoms to an As-O layer. This is important as it prevents the mixed oxide from forming; the mixed As-O-Si oxide layer is not observed in the As-rich case (see Fig. 1). For both the As-rich and As-lean cases, the oxide formation mechanisms are “self-limiting” in that the stoichiometry of the films is prescribed which effectively can fix the concentration of species at critical interfaces. Finally, we note that hydrogen could interact with the surface during or after the plasma process, which might affect plasma doping. However, our experiments show that the film formation does not change significantly with hydrogen added in process, and thus the effect of hydrogen was excluded in this work; but it is a focus of ongoing research.

We acknowledge the generous support of the Welch Foundation (F-1535) for G.S.H. and also the Texas Advanced Computing Center for use of their computing resources.

¹A. Agarwal, in *Proceedings of the IEEE International Conference on Ion Implantation Technology*, Piscataway, NJ (2000), p. 293.

²N. Cheung, *Mater. Chem. Phys.* **46**, 132 (1996).

³*Handbook of Plasma Immersion: Ion Implantation and Deposition*, edited by A. Anders (Wiley, New York, 2000).

⁴Y. Sasaki, C. G. Jin, H. Tamura, B. Mizuno, R. Higaki, T. Satoh, K. Majima, H. Saoudin, K. Takagi, S. Ohmi, K. Tsutsui, and H. Iwai, *Symp. on VLSI Tech. Dig.* 180 (2004).

⁵Y. Sasaki, H. Ito, K. Okashita, H. Tamura, C. G. Jin, B. Mizuno, T. Okumura, I. Aib, Y. Fukagaw, H. Saoudin, K. Tsutsui, and H. Iwai, *AIP Conf. Proc.*, 16th International Conference on Ion Implantation Technology (IIT 2006), 524 (2006).

⁶Y. Sasaki, K. Okashita, K. Nakamoto, T. Kitaoka, B. Mizuno, and M. Ogura, *Tech. Dig. IEDM* 917 (2008).

⁷Y. Sasaki, K. Okashita, S. Hayashi, K. Nakamoto, T. Kitaoka, B. Mizuno, M. Kubota, M. Ogura, and O. Nishijima, in *Symposium on Dry Process* (2010), Paper No. F-1, p. 103.

⁸M. Ritala and M. Leskelä, *Handbook of Thin Film Materials* (Academic, San Diego, CA, 2002), Vol. 1.

⁹K. Kobayashi, T. Eto, K. Okuyama, K. Shibahara, and H. Sunami, *Jpn. J. Appl. Phys., Part 1* **44**(4B), 2273 (2005).

¹⁰C. Steen, A. Martinez-Limia, P. Pichler, H. Ryssel, S. Paul, W. Lerch, L. Pei, G. Duscher, F. Severac, F. Cristiano, and W. Windl, *J. Appl. Phys.* **104**, 023518 (2008).

¹¹H. Ueda, P. L. G. Ventzek, M. Oka, M. Horigome, Y. Kobayashi, Y. Sugimoto, T. Nozawa, and S. Kawakami, *J. Appl. Phys.* **115**, 214904 (2014).

¹²M. A. Berding and A. Sher, *Phys. Rev. B* **58**, 3853 (1998).

¹³W. Luo, P. B. Rasband, P. Clancy, and B. W. Roberts, *J. Appl. Phys.* **84**, 2476 (1998).

¹⁴S. Harrison, T. Edgar, and G. S. Hwang, *Phys. Rev. B* **74**, 195202 (2006).

¹⁵S. Harrison, T. Edgar, and G. S. Hwang, *Appl. Phys. Lett.* **87**, 231905 (2005); *Electrochem. Solid-State Lett.* **9**, G354 (2006).

¹⁶R. Kögler, E. Wieser, J. Albrecht, and P. Knothe, *Phys. Status Solidi A* **113**, 321 (1989).

¹⁷S. Whelan, V. Privitera, G. Mannino, M. Italia, C. Bongiorno, E. Napolitani, E. J. H. Collart, and J. A. van den Berg, *Nucl. Instrum. Methods Phys. Res., Sect. B* **186**, 271 (2002).

¹⁸G. K. Celler, L. E. Trimble, T. T. Sheng, K. W. West, S. G. Kosinski, and L. Pfeiffer, in *SiO₂ and Its Interfaces*, edited by G. Lucovsky and S. T. Pantelides (Mater. Res. Soc. Symp. Proc., 1988), Vol. 105, p. 47.

¹⁹Y. Tsunashima and N. Aoki, *Tech. Dig. IEDM* 699 (1997).

- ²⁰Y. Wada and D. A. Antoniadis, *J. Electrochem. Soc.* **128**, 1317 (1981).
- ²¹S. Alexandrova, *J. Appl. Phys.* **78**, 1514 (1995).
- ²²L. L. Raja, S. Mahadevan, P. L. G. Ventzek, and J. Yoshikawa, *J. Vac. Sci. Technol., A* **31**, 031304 (2013).
- ²³J. P. Perdew, K. Burke, and M. Ernzerhof, *Phys. Rev. Lett.* **77**, 3865 (1996).
- ²⁴G. Kresse and J. Furthmüller, *VASP: The Guide* (Vienna University of Technology, Vienna, Austria, 2001).
- ²⁵P. E. Blöchl, *Phys. Rev. B* **50**, 17953 (1994).
- ²⁶H. J. Monkhorst and J. D. Pack, *Phys. Rev. B* **13**, 5188 (1976).
- ²⁷A. F. Wells, *Structural Inorganic Chemistry* (Oxford University Press, London, England, 1984).
- ²⁸M. Eagleson, *Concise Encyclopedia Chemistry* (de Gruyter, Berlin, 1994).
- ²⁹P. Ballirano and A. Maras, *Z. Kristallogr. NCS* **217**, 177 (2002).
- ³⁰A. J. Frueh, *J. Am. Mineral.* **36**, 833 (1951).
- ³¹F. Pertlik, *Monatsh. Chem.* **106**, 755 (1975).
- ³²S. Lee, R. J. Bondi, and G. S. Hwang, *Phys. Rev. B* **84**, 045202 (2011).
- ³³S. Lee, R. J. Bondi, and G. S. Hwang, *J. Appl. Phys.* **109**, 113519 (2011).
- ³⁴R. M. Van Ginhoven, H. Jonsson, and L. R. Corrales, *Phys. Rev. B* **71**, 024208 (2005).
- ³⁵See supplementary material at <http://dx.doi.org/10.1063/1.4905206> for the cluster models that we employed in the oxidation state and penalty energy calculations of As and Si in the As-Si-O system.